Neural Computing and Applications (2020) 32:4317–4323
https://doi.org/10.1007/s00521-018-03968-y

COGNITIVE COMPUTING FOR INTELLIGENT APPLICATION AND SERVICE

An LBP encoding scheme jointly using quaternionic representation and angular information

Rushi Lan[1,2] · Huimin Lu[3] · Yicong Zhou[4] · Zhenbing Liu[5] · Xiaonan Luo[5]

Received: 13 July 2018 / Accepted: 20 December 2018 / Published online: 4 January 2019

Abstract
Local descriptors play a crucial role in numerous computer vision and pattern recognition applications. This paper proposes a novel local descriptor, called the quaternionic local angular binary pattern (QLABP), for color image classification. QLABP is based on the quaternionic representation (QR) of color images such that it is able to handle all color components holistically as well as consider their relations. Using QR, the quaternionic angular information is further developed to account for more color characteristics. We provide two ways to derive the quaternionic angular information from different perspectives. A pattern encoding operation is finally conducted on the obtained angular information to obtain QLABP. The effectiveness of QLABP has successfully been evaluated by comparing with several state-of-the-art descriptors.

Keywords Quaternionic representation (QR) · Local binary pattern (LBP) · Quaternionic angular information · Image classification

1 Introduction

Local descriptors are widely used features in the fields of computer vision and pattern recognition [5, 10, 32, 33, 38]. A large number of local descriptors have been proposed from different perspectives so far. Among existing local descriptors, the local binary pattern (LBP) [26] has been regarded as one of the most successful and popular characteristics because of its impressive performance in many practical applications. Considerable effort has been devoted to improving the discriminative capabilities and robustness of LBP from different perspectives. Representative LBP variants include completed LBP (CLBP) [12], robust LBP (RLBP) [25], local ternary patterns (LTP) [31], discriminative robust LBP (DRLBP) [29], quaternionic local ranking binary pattern (QLRBP) [18], and quaternionic Michelson contrast binary pattern (QMCBP) [17], etc.

With the rapid development of imaging equipment, more attention has been paid to extracting local features from color images. A common strategy is to perform the aforementioned LBP-based approaches to each color channel individually and then concatenate the derived features together to form a final feature vector. However, such a strategy does not take the relations among different color channels into account, which contain valuable information that will benefit the classification performance. To solve this kind of problem, Lee et al. [21] proposed a local color vector binary pattern (LCVBP) for color images, which considers the relation between two color channels by their ratio. The authors in [16] developed a method that converts an image into a graph and explored the shortest paths to discover the relations among color channels. Satisfactory results were achieved.

✉ Huimin Lu
dr.huimin.lu@ieee.org

Rushi Lan
rslan2016@163.com

1 School of Computer Science and Engineering, South China University of Technology, Guangzhou, China

2 Guangxi Key Laboratory of Intelligent Processing of Computer Image and Graphics, Guilin University of Electronic Technology, Guilin, China

3 Department of Mechanical and Control of Engineering, Kyushu Institute of Technology, Kitakyushu, Japan

4 Department of Computer and Information Science, University of Macau, Macao, China

5 Guangxi Key Laboratory of Trusted Software, Guilin University of Electronic Technology, Guilin, China

To efficiently consider the interactions between color channels, a color image representation, termed quaternionic representation (QR) [6, 7, 19], has been utilized to derive local descriptors. QR exploits a quaternion to encode all color channels such that it handles them in a holistic manner and includes their relations simultaneously. A quaternionic LBP (QLBP) [20] and its extended version QLRBP were proposed by combining both advantages of QR and LBP. Comparison results have shown that QLRBP outperforms LBP and some of its improved versions. QLBP performs LBP on the phase image of the Clifford translation (CT) transformed result to extract local descriptors. Compared with the ratio of the two color channels used in LCVBP, this phase consists of more discriminative characteristics among the color channels. However, QLBP and QLRBP just take one phase into account to derive features. It is interesting to further consider the interactions between different phases to obtain local descriptors.

In this paper, we propose a novel local descriptor, named the quaternionic local angular binary pattern (QLABP), for color image classification. QLABP is derived in the quaternion domain such that it takes advantage of QR for color images. Compared with QLBP and QLRBP in which local descriptors are extracted from one phase, QLABP involves a quaternionic angular that is developed to consider the relations between two phases such that it contains more comprehensive color characteristics. A pattern encoding procedure is finally conducted on the quaternionic angular to achieve the QLABP descriptor. The comparison results on three representative texture databases demonstrate the effectiveness of QLABP.

The remainder of the paper is organized as follows. Section 2 introduces the related mathematical background about quaternion algebra. Section 3 describes the proposed QLABP algorithm in detail. In Sect. 4, several experiments are carried out to evaluate QLABP. Section 5 presents our conclusions.

2 Quaternion algebra

As a 4D generation of the traditional 2D complex number system, a quaternion $\dot{q}$ consists of one real part and three imaginary parts as follows [8, 13]:

$$\dot{q} = q + ai + bj + ck, \tag{1}$$

where q, a, b, and c are real numbers, and $\{i, j, k\}$ are the basic imaginary units that satisfy the following relationships, respectively.

$$i^2 = j^2 = k^2 = ijk = -1,$$
$$ij = -ji = k, \quad jk = -kj = i, \quad ki = -ik = j.$$

q is the real part of $\dot{q}$, and $ai + bj + ck$ is the imaginary part. If $q = 0$, $\dot{q}$ is a pure quaternion.

Several basic properties of quaternion algebra can be similarly derived as the complex number system. For instance, the conjugate, modulus, and inverse of $\dot{q}$ are defined as follows, respectively:

$$\dot{q}^* = q - (ai + bj + ck), \tag{2}$$

$$|\dot{q}| = \sqrt{\dot{q}\dot{q}^*} = \sqrt{q^2 + a^2 + b^2 + c^2}, \tag{3}$$

$$\dot{q}^{-1} = \frac{\dot{q}^*}{|\dot{q}|^2}. \tag{4}$$

Note that $\dot{q}$ is a unit quaternion if $|\dot{q}| = 1$. For simplicity, we represent the real and imaginary parts of $\dot{q}$ by $S(\dot{q})$ and $V(\dot{q})$. Equation (1) can be converted to a polar version as:

$$\dot{q} = |\dot{q}|e^{\dot{\mu}\theta} = |\dot{q}|(\cos\theta + \dot{\mu}\sin\theta), \tag{5}$$

where $\dot{\mu} = \frac{V(\dot{q})}{|V(\dot{q})|}$ and $\theta = \tan^{-1}\frac{|V(\dot{q})|}{S(\dot{q})}$. $\dot{\mu}$ is known as the eigenaxis of $\dot{q}$, and θ is the phase (or eigenangle). In the following, we will use $\theta(\cdot)$ as an operator to extract the phase of a quaternion. More details about quaternion algebra can be found in [7, 13].

3 Methodology

This section details the proposed QLABP descriptor. Figure 1 illustrates a schematic picture of the QLABP descriptor, which consists of three key steps, namely QR of color images, quaternionic angular information extraction, and pattern encoding, respectively. In the following section, we will present these steps successively.

3.1 QR of color images

To handle the color image in the quaternionic domain, the first step is to represent it by quaternions. However, the color image is usually described in the RGB color space, which is a 3D space, while the quaternion is a 4D number

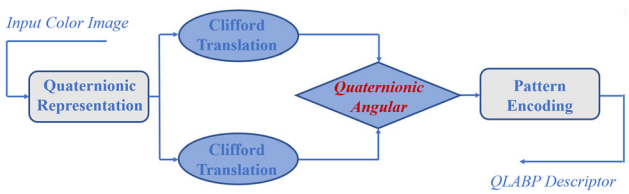

Fig. 1 A schematic picture of the quaternionic local angular binary pattern (QLABP) descriptor

system. To remove this mismatch, the imaginary parts of a quaternion are used to represent a color pixel as [7]:

$$\dot{Q}(x,y) = R(x,y)i + G(x,y)j + B(x,y)k, \tag{6}$$

where $\dot{Q}(x,y)$ is the QR of the color pixel, and $R(x, y)$, $G(x, y)$, and $B(x, y)$ are the red, green, and blue components of a color pixel, respectively. $\dot{Q}(x,y)$ provides a one-to-one mapping between the quaternionic domain and the RGB color space. Any operations to $\dot{Q}(x,y)$ will affect all the color channels such that the interactions among the different channels will be considered simultaneously.

3.2 Angular information extraction in the quaternion domain

Using the QR, the color image is represented by a quaternionic matrix whose elements are quaternion numbers. In the following section, we will present two methods for extracting the angular information in the quaternion domain.

3.2.1 Quaternion-based angular information (QAI)

Inspired by LCVBP that is derived from the ratio of two color channels, it is natural to extract the angular information using two quaternions. To this end, it is necessary to generate two other quaternionic matrices from the QR of the color image first. Here, we consider the Clifford transform (CT) [20], a commonly used operator to transform a quaternion to another quaternion, to derive the angular information. Let $\dot{P} = \alpha i + \beta j + \gamma k$ be a pure unit quaternion ($|\dot{P} = 1|$). The CT of $\dot{Q}$ in Eq. (6) by $\dot{P}$ is defined as follows:[1]

$$\begin{aligned} \mathrm{CT}\ (\dot{Q},\dot{P}) = \dot{Q}\dot{P} = &-(R\alpha + G\beta + B\gamma) + (G\gamma - B\beta)i \\ &+ (B\alpha - R\gamma)j + (R\beta - G\alpha)k. \end{aligned} \tag{7}$$

The coefficients of $\mathrm{CT}\ (\dot{Q},\dot{P})$ measure the differences between $\{R, G, B\}$ and $\{\alpha, \beta, \gamma\}$. Let $\dot{P}_1 = \alpha_1 i + \beta_1 j + \gamma_1 k$ and $\dot{P}_2 = \alpha_2 i + \beta_2 j + \gamma_2 k$ ($\dot{P}_1 \neq \dot{P}_2$) be two pure unit quaternions. Hence, $\mathrm{CT}\ (\dot{Q},\dot{P}_1)$ and $\mathrm{CT}\ (\dot{Q},\dot{P}_2)$ highlight the different characteristics of $\dot{Q}$. Then, the developed QAI, denoted by Λ_2^1 here, is defined as follows:

$$\Lambda_2^1 = \theta\left(\frac{\mathrm{CT}(\dot{Q},\dot{P}_1)}{\mathrm{CT}(\dot{Q},\dot{P}_2)}\right), \tag{8}$$

where $\theta(\cdot)$ is the phase of a quaternion. It can be seen that Λ_2^1 is derived from the ratio of two quaternions. Compared with LCVBP, which is based on the ratio of two color channels, $\frac{\mathrm{CT}(\dot{Q},\dot{P}_1)}{\mathrm{CT}(\dot{Q},\dot{P}_2)}$ accounts for many comprehensive color characteristics. The $\theta(\cdot)$ is used to convert $\frac{\mathrm{CT}(\dot{Q},\dot{P}_1)}{\mathrm{CT}(\dot{Q},\dot{P}_2)}$ from the quaternion domain to real domain that will be more convenient for feature extraction.

3.2.2 Phase-based angular information (PAI)

The phase of a quaternion describes the relation between the coefficients of the real and imaginary parts. Considering the Clifford transform in Eq. (7), its phase Φ can be achieved by:

$$\Phi = \tan^{-1}\frac{\sqrt{(G\gamma - B\beta)^2 + (B\alpha - R\gamma)^2 + (R\beta - G\alpha)^2}}{-(R\alpha + G\beta + B\gamma)}. \tag{9}$$

Our previous studies have shown that Φ takes more complex relations between different channels into account [18]. $\dot{P}$ is regarded as a reference quaternion in this situation. Φ will be large if $\dot{Q}$ and $\dot{P}$ are more similar to each other. More discussions about the phase of the CT result can be found in [20, 34].

In the phase extraction stage, CT is performed to each pixel of the image by the same reference quaternion. The image characteristics, which are similar to the reference quaternion $\dot{P}$, are highlighted. We can comprehensively explore the image features by applying several reference quaternions. In order to strengthen the representation ability, it is necessary to further consider the interaction between different phases. Inspired by the LCVBP descriptor, we propose a quaternionic angular to represent the relation between two phases. Let $\Phi_{\dot{P}_1}$ and $\Phi_{\dot{P}_2}$ be two phases derived by two different quaternions $\dot{P}_1 = \alpha_1 i + \beta_1 j + \gamma_1 k$ and $\dot{P}_2 = \alpha_2 i + \beta_2 j + \gamma_2 k$. The phase-based angular information (PAI), denoted by Λ_2^1, is defined as follows:

$$\Lambda_2^1 = \tan^{-1}\frac{\Phi_{\dot{P}_1}}{\Phi_{\dot{P}_2}}. \tag{10}$$

To provide an in-depth analysis of Λ_2^1, we substitute $\Phi_{\dot{P}_1}$ and $\Phi_{\dot{P}_2}$ into $\frac{\Phi_{\dot{P}_1}}{\Phi_{\dot{P}_2}}$ resulting in:

$$\frac{\Phi_{\dot{P}_1}}{\Phi_{\dot{P}_2}} = \frac{\tan^{-1}\frac{\sqrt{(G\gamma_1 - B\beta_1)^2 + (B\alpha_1 - R\gamma_1)^2 + (R\beta_1 - G\alpha_1)^2}}{-(R\alpha_1 + G\beta_1 + B\gamma_1)}}{\tan^{-1}\frac{\sqrt{(G\gamma_2 - B\beta_2)^2 + (B\alpha_2 - R\gamma_2)^2 + (R\beta_2 - G\alpha_2)^2}}{-(R\alpha_2 + G\beta_2 + B\gamma_2)}}. \tag{11}$$

Note that $\tan^{-1} x$ can be represented using the following series representation:

[1] Note that there are two types of CT for a quaternion, namely the left CT and right CT, and their phases are equal. We use the right CT as in Eq. (7) to illustrate the derivation of QLABP in this paper.

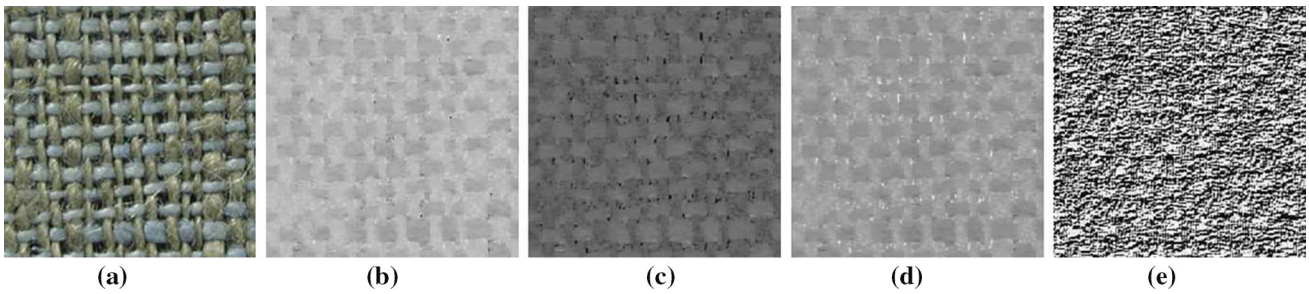

Fig. 2 Illustration of extracting QLABP from a color texture image. **a** An example of a color texture image. **b**, **c** The phase image extracted by using i and j as reference quaternions. **d** The quaternionic angular derived from the two phase images. **e** The LBP encoding result from the phase angle image

$$\tan^{-1} x = \frac{x}{1+x^2} \sum_{n=0}^{\infty} \prod_{s=1}^{n} \frac{2lx^2}{(2l+1)(1+x^2)}. \tag{12}$$

Combining Eqs. (9) and (12) together, we can derive:

$$\Phi_{\dot{P}_l} = \frac{-\omega_l \sqrt{v_l}}{v_l + \omega_l^2} \varphi_l, \tag{13}$$

where $l \in \{1,2\}, v_l = (G\gamma_l - B\beta_l)^2 + (B\alpha_l - R\gamma_l)^2 + (R\beta_l - G\alpha_l)^2$, $\omega_l = R\alpha_l + G\beta_l + B\gamma_l$, and $\varphi_l = \sum_{n=0}^{\infty} \prod_{s=1}^{n} \frac{2sv_l}{(2s+1)(v_l+\omega_l^2)}$. It can be seen that v_l and ω_l describe the similarity of $\dot{Q}$ and $\dot{P}_l$ from different aspects, namely v_l denotes the difference of the cross-multiplications of two color components, and ω_l applies the inner product to represent the similarity. Using Eq. (13), we can rewrite Eq. (11) as:

$$\frac{\Phi_{\dot{P}_1}}{\Phi_{\dot{P}_2}} = \frac{\omega_1 \sqrt{v_1}}{\omega_2 \sqrt{v_2}} \cdot \frac{\omega_2^2 + v_2}{\omega_1^2 + v_1} \cdot \frac{\varphi_1}{\varphi_2}. \tag{14}$$

We can observe that Eq. (14) exploits various combinations of v_l and ω_l to describe the relations between $\dot{Q}$ and $\dot{P}_l$. More comprehensive relations between color components can be explored using different $\dot{P}_l$.

3.3 QLABP

Although the quaternionic angular can be directly applied as a feature for color images, we further perform a pattern encoding operation to make the achieved descriptors more robust and discriminative. LBP has been proven to be a simple yet quite efficient method to describe the local characteristics; therefore, we conduct an LBP coding to the quaternionic angular information of the QR of the color images. Hence, the derived feature is called the quaternionic local angular binary pattern (QLABP). Figure 2 also illustrates the derivation of QLABP for a color image. To comprehensively capture the image characteristics, we further utilize the 2D joint histogram of two QLABP encoding results as the final feature representation for color images.

4 Experimental results

In this section, several experiments will be carried out to evaluate the performance of the proposed QLABP descriptor for color image classification. The setting of all experiments is first given, and the results on the used datasets are presented successively. Finally, a discussion on time complexity is provided.

4.1 Experimental setting

Three representative texture databases, namely KTH-TIPS2-a [15], KTH-TIPS [15], and USPTex [1], are chosen for evaluation. The detailed information of these datasets, including the number of classes, number of each class, and the total number of images, is listed in Table 1. Some example texture images of these datasets are shown in Fig. 3. In this work, three pairs of reference quaternions, namely (i, j), (i, k), and (j, k), are chosen to generate the QLABP descriptor. Three 2D joint histograms, derived from $\{\text{QLABP}_{i,j}, \text{QLABP}_{i,k}\}$, $\{\text{QLABP}_{i,j}, \text{QLABP}_{j,k}\}$, and $\{\text{QLABP}_{i,k}, \text{QLABP}_{j,k}\}$ respectively, are concentrated to form a feature vector for classification. Here, we apply QLABP_q and QLABP_p to denote the features that are

Table 1 Image datasets used for evaluation

Dataset name	No. of classes	No. of each class	Total images
KTH-TIPS2-a	11	Vary	4395
KTH-TIPS	10	81	810
USPTex	191	12	2292

Fig. 3 Sample images of color texture images used in the experiments. The images in the first to third rows are randomly chosen from the KTH-TIPS2-a, KTH-TIPS, and USPTex datasets, respectively

Table 2 Classification results (%) of KTH-TIPS2-a dataset using different features

Methods	KTH-TIPS2-a dataset
LBP [26]	58.2
WLD [4]	61.0
LCVBP [21]	61.5
QLBP [20]	61.7
DRLBP [29]	59.0
DRLTP [29]	62.6
QLRBP [18]	64.5
$QLABP_q$	61.4
$QLABP_p$	**65.4**

The best result is in bold

extracted via the quaternion-based angular information and phase-based angular information, respectively.

4.2 KTH-TIPS2-a dataset

This dataset consists of 11 materials, such as cork, cracker, and linen, etc. Note that the images that are 200×200 in size are selected for evaluation, and the total number of images is 4395. For each material, the images are captured in various scales, illumination directions, and poses. In this test, the following local descriptors are chosen for evaluation: LBP [26], WLD [4], LCVBP [21], QLBP [20], DRLBP [29], DRLTP [29], and QLRBP [18], respectively. The experiment here is identically set as that applied in the literature [4, 29]. The classification performance of all methods is reported in Table 2. We can observe that WLD, LCVBP, and QLBP achieve similar performance, and they work better than LBP and DRLBP. For this dataset, the performance of $QLABP_q$ is comparable with that of LCVBP and QLBP. $QLABP_p$ outperforms $QLABP_q$ by 4% and also surpasses other comparative features by different degrees.

4.3 KTH-TIPS dataset

This dataset includes ten classes of texture images, and there are 81 images for each class. All images in this dataset are 200×200 in size. In this experiment, the proposed QLABP is compared with the schemes in [3, 11], LBP [26], LCVBP [21], WLD [4], QLBP [20], and QLRBP [18], respectively. As in [11], the experiment is carried out by the leave-one-out strategy, and the nearest neighbor (NN) classifier is applied. Table 3 illustrates the classification rates of all test approaches. It can be seen that the local descriptors surpass the CK-1 and sparse algorithms proposed in [3, 11]. Among the local descriptors, the classification rate of LBP is slightly smaller than that of the other descriptors. The performances of LCVBP, WLD, and QLBP are similar in this case. $QLABP_p$ and QLRBP obtain the same results here, and they both outperform $QLABP_q$.

Table 3 Classification results (%) of the KTH-TIPS dataset using different features

Methods	KTH-TIPS dataset
CK-1 [3]	86.00
Sparse [11]	84.50
LBP [26]	93.83
LCVBP [21]	96.54
WLD [4]	97.28
QLBP [20]	97.41
QLRBP [18]	**98.64**
$QLABP_q$	95.56
$QLABP_p$	**98.64**

The best results are in bold

Table 4 Classification results (%) of the USPTex dataset using different features

Methods	USPTex dataset
Average RGB	36.19
LBP + Haralick [28]	73.17
MSD [22]	51.29
Multilayer CCR [2]	82.08
HRF [27]	49.86
Gabor EEE [14, 30]	92.58
Shortest Graph [16]	66.71
LBP [26]	87.84
LCVBP [21]	92.48
WLD [4]	92.34
QLBP [20]	84.82
QLRBP [18]	86.74
$QLABP_q$	85.96
$QLABP_p$	**93.80**

The best result is in bold

4.4 USPTex dataset

This dataset has 191 classes of texture images, and each class contains 12 images with a size of 128×128. Apart from the LBP, LCVBP, WLD, QLBP, and QLRBP methods, the following schemes are selected for comparison: average RGB, LBP + Haralick [28], MSD [22], Multilayer CCR [2], HRF [27], Gabor EEE [14, 30], and shortest graph [16]. As in the literature, the experiment here is set as follows. For each class, two-thirds of the images are randomly selected to use as the training set, and the remaining images are regarded as the testing set. The NN classifier is applied, and the average rate of ten runs is utilized as the classification result of each method. Table 4 lists the performance of all the methods. It can be seen that Gabor EEE, LCVBP, WLD, and QLABP approaches obtain more satisfactory results for this dataset. QLBP performs worse than LBP by approximately three percent, and QLRBP also does not perform very well too. Compared with QLBP and QLRBP, $QLABP_p$ considers more color characteristics such that it obtains a significant improvement and surpasses all the other methods.

Table 5 Average running times (in seconds) of LBP, $QLABP_q$, and $QLABP_p$ to color images with a size 512×512

Methods	Running time
LBP	0.1170
$QLABP_q$	0.1941
$QLABP_p$	0.1753

4.5 Time complexity analysis

In this part, we study the time complexity of QLABP. Compared with the original LBP, the proposed QLABP further carries out the following operations: quaternionic representation of an input color image and angular information extraction. These two operations are conducted matrixwise such that they are not time-consuming. Here, we conduct $QLABP_q$, $QLABP_p$, and LBP to 100 color images whose sizes are resized to 512×512. Note that LBP is performed to the grayscale version of the corresponding color images. The average running times of all the methods are reported in Table 5. It can be seen that among the three methods, LBP requires the least running time, while $QLABP_q$ is the most time-consuming. Although $QLABP_q$ and $QLABP_p$ need approximately 0.08 and 0.06 s additionally, they are all with same time complexity with LBP.

5 Conclusion

We have presented a novel quaternionic local descriptor (the QLABP) for image classification. Compared with conventional local descriptors, QLABP is based on the QR of the color image such that it takes advantage of the superiorities of QR. Additionally, QLABP considers more color characteristics in comparison with QLBP. Experiments on three representative databases (i.e., KTH-TIPS2-a, KTH-TIPS, and USPTex) clearly demonstrated that QLABP achieved better performance than several state-of-the-art local descriptors for color texture classification. In the future, to further improve the performance of QLABP, the well-known feature learning schemes, such as [9, 23, 24, 35–37], can be used in the QLABP framework to derive more robust and discriminative features for color images.

Acknowledgements This work was partially supported by the National Natural Science Foundation of China (Nos. 61702129, 61772149, U1701267, and 61320106008), China Postdoctoral Science Foundation (No. 2018M633047), Guangxi Science and Technology Project (No. 2018AD19029), the Macau Science and Technology Development Fund under Grant FDCT/189/2017/A3, and by the Research Committee at University of Macau under Grants MYRG2016-00123-FST and MYRG2018-00136-FST.

Compliance with ethical standards

Conflict of interest The authors declare that they have no conflict of interest.

References

1. Backes AR, Casanova D, Bruno OM (2012) Color texture analysis based on fractal descriptors. Pattern Recognit 45(5):1984–1992
2. Bianconi F, Fernández A, González E et al (2009) Rotation-invariant colour texture classification through multilayer CCR. Pattern Recognit Lett 30(8):765–773
3. Campana L, Keogh J (2010) A compression-based distance measure for texture. Stat Anal Data Min ASA Data Sci J 3(6):381–398
4. Chen J, Shan S, He C et al (2010) WLD: a robust local image descriptor. IEEE Trans Pattern Anal Mach Intell 32(9):1705–1720
5. Chhabra P, Garg NK, Kumar M (2018) Content-based image retrieval system using ORB and SIFT features. Neural Comput Appl. https://doi.org/10.1007/s00521-018-3677-9
6. Ell T (1992) Hypercomplex spectral transforms. PhD dissertation, University of Minnesota, Minneapolis
7. Ell T, Sangwine S (2007) Hypercomplex Fourier transforms of color images. IEEE Trans Image Process 16(1):22–35
8. Gai S, Wan MH, Wang L, Yang CH (2014) Reduced quaternion matrix for color texture classification. Neural Comput Appl 25(3–4):945–954
9. Gao L, Guo Z, Zhang H, Xu X, Shen HT (2017) Video captioning with attention-based lstm and semantic consistency. IEEE Trans Multimed 19(9):2045–2055
10. Geng T, Yang M, You Z, Cai Y, Huang F (2018) Multiscale overlapping blocks binarized statistical image features descriptor with flip-free distance for face verification in the wild. Neural Comput Appl 30(10):3243–3252
11. Guha T, Ward RK (2014) Image similarity using sparse representation and compression distance. IEEE Trans Multimed 16(4):980–987
12. Guo Z, Zhang L, Zhang D (2010) A completed modeling of local binary pattern operator for texture classification. IEEE Trans Image Process 19(6):1657–1663
13. Hamilton WR, Hamilton WE (1866) Elements of quaternions. Longmans, Green, & Company, London
14. Hoang MA, Geusebroek JM, Smeulders AWM (2005) Color texture measurement and segmentation. Signal Process 85(2):265–275
15. http://www.nada.kth.se/cvap/databases/kth-tips/. Accessed 1 Oct 2014
16. Junior J, Cortez C, Backes R (2014) Color texture classification using shortest paths in graphs. IEEE Trans Image Process 23(9):3751–3761
17. Lan R, Zhou Y (2016) Quaternion-Michelson descriptor for color image classification. IEEE Trans Image Process 25(11):5281–5292
18. Lan R, Zhou Y, Tang YY (2016) Quaternionic local ranking binary pattern: a local descriptor of color images. IEEE Trans Image Process 25(2):566–579
19. Lan R, Zhou Y, Tang YY (2017) Quaternionic weber local descriptor of color images. IEEE Trans Circuits Syst Video Technol 27(2):261–274
20. Lan R, Zhou Y, Tang YY, Chen CLP (2014) Person reidentification using quaternionic local binary pattern. In: IEEE international conference on multimedia and expo (ICME), pp 1–6
21. Lee SH, Choi JY, Ro YM, Plataniotis KN (2012) Local color vector binary patterns from multichannel face images for face recognition. IEEE Trans Image Process 21(4):2347–2353
22. Liu G, Li Z, Zhang L, Xu Y (2011) Image retrieval based on micro-structure descriptor. Pattern Recognit 44(9):2123–2133
23. Lu H, Li B, Zhu J, Li Y, Li Y, Xu X, He L, Li X, Li J, Serikawa S (2017) Wound intensity correction and segmentation with convolutional neural networks. Concurr Comput Pract Exp 29(6):e3927
24. Lu H, Li Y, Uemura T, Ge Z, Xu X, He L, Serikawa S, Kim H (2017) Fdcnet: filtering deep convolutional network for marine organism classification. Multimed Tools Appl 77(17):21847–21860
25. Nguyen D, Zong Z, Ogunbona P, Li W (2010) Object detection using non-redundant local binary patterns. In: 17th IEEE international conference on image processing (ICIP), pp 4609–4612
26. Ojala T, Pietikainen M, Maenpaa T (2002) Multiresolution gray-scale and rotation invariant texture classification with local binary patterns. IEEE Trans Pattern Anal Mach Intell 24(7):971–987
27. Paschos G, Petrou M (2003) Histogram ratio features for color texture classification. Pattern Recognit Lett 24(1):309–314
28. Porebski A, Vandenbroucke N, Macaire L (2008) Haralick feature extraction from LBP images for color texture classification. In: First workshops on image processing theory, tools and applications, pp 1–8
29. Satpathy A, Jiang X, Eng H (2014) LBP based edge-texture features for object recognition. IEEE Trans Image Process 23(5):1953–1963
30. Swain MJ, Ballard DH (1991) Color indexing. Int J Comput Vis 7(1):11–32
31. Tan X, Triggs B (2010) Enhanced local texture feature sets for face recognition under difficult lighting conditions. IEEE Trans Image Process 19(6):1635–1650
32. Wang D, Lu H, Li X (2011) Two dimensional principal components of natural images and its application. Neurocomputing 74(17):2745–2753
33. Wang D, Lu H, Yang MH (2015) Kernel collaborative face recognition. Pattern Recognit 48(10):3025–3037
34. Weeks J, Lehoucq R, Uzan JP (2003) Detecting topology in a nearly flat spherical universe. Class Quantum Gravity 20(8):1529
35. Xu X, He L, Lu H, Gao L, Ji Y (2018) Deep adversarial metric learning for cross-modal retrieval. World Wide Web. https://doi.org/10.1007/s11280-018-0541-x
36. Xu X, He L, Shimada A, Taniguchi R, Lu H (2016) Learning unified binary codes for cross-modal retrieval via latent semantic hashing. Neurocomputing 213:191–203
37. Xu X, Shen F, Yang Y, Shen HT, Li X (2017) Learning discriminative binary codes for large-scale cross-modal retrieval. IEEE Trans Image Process 26(5):2494–2507
38. Yang M, Qian YQ, Xue LJ, Li H, Deng LY, Wang CX (2018) G2P: a new descriptor for pedestrian detection. Neural Comput Appl. https://doi.org/10.1007/s00521-018-3815-4